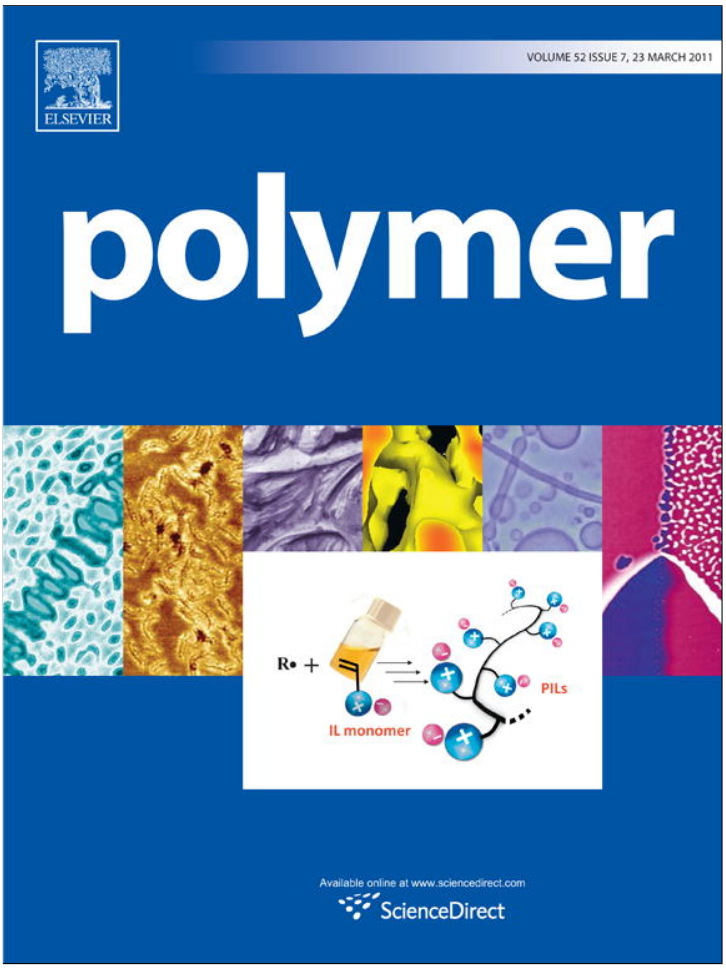

Polymer 52 (2011) 1654–1661

Contents lists available at ScienceDirect

Polymer

journal homepage: www.elsevier.com/locate/polymer

# Characterization and modeling of direct-write fabrication of microscale polymer fibers

Scott M. Berry [a,b,1], Santosh Pabba [b,2], Jérôme Crest [c], Scott D. Cambron [a,d], Gareth H. McKinley [c], Robert W. Cohn [b], Robert S. Keynton [a,b,d,*]

[a] Department of Mechanical Engineering, 200 Sacket Hall, University of Louisville, Louisville, KY 40292, USA
[b] The Electro Optics Research Institute & Nanotechnology Center, University of Louisville, Louisville, KY 40292, USA
[c] Department of Mechanical Engineering, 3-250, Massachusetts Institute of Technology, Cambridge, MA 02139, USA
[d] Department of Bioengineering, 419 Lutz Hall, University of Louisville, Louisville, KY 40292, USA

ARTICLE INFO

*Article history:*
Received 9 November 2010
Received in revised form
23 January 2011
Accepted 30 January 2011
Available online 28 February 2011

*Keywords:*
Direct-write
Elongational flow
Polymer microfibers

ABSTRACT

A new direct-write system for fabricating suspended microscale and sub-microscale polymer fibers has been developed and characterized. This system is capable of generating arrays of precisely-positioned fibers with controllable diameters in three-dimensional space. The driving mechanism behind this process harnesses the surface tension of liquid bridges to promote the controlled thinning of a macroscale polymer solution filament into the desired micro- or sub-microscale fiber. The correlation between fiber diameter and several experimental parameters including solution concentration, drawing rate, and fiber length was characterized using a series of viscous poly(methyl methacrylate) (PMMA) solutions. A dimensional analysis of the physics of the fiber drawing process was used to adapt this data into an empirical relationship describing fiber formation from a generalized polymer solution. This information was subsequently utilized to predict fiber diameter from several other non-PMMA-based polymer solutions with accuracy comparable to the intrinsic variation of the process itself, thereby eliminating the need to perform lengthy characterizations on new polymer solutions.



## 1. Introduction

Polymeric materials have received much interest within the field of microscale fabrication due to their versatility and customizability. Creative polymer syntheses have facilitated the creation of advanced materials with a diversity of novel mechanical, chemical, electrical, and biological properties. These distinctive attributes have prompted the development of a myriad of devices including sensors [1,2], cellular scaffolds [3–8], and microelectronic components [9,10]. An emergent theme in the design of such devices has been the selection of micro- and nanofibrous architectures, as these configurations have been demonstrated to improve both device performance and mechanical robustness/flexibility. These improvements stem from several advantageous qualities which are intrinsic to such geometries, including three-dimensionality, abundant polymer surface area, and increased strength and flexibility relative to bulk polymer materials.

A variety of fiber fabrication techniques, including wet spinning, dry spinning, and electrospinning, are currently utilized to produce polymer fibers [11]. However, shortcomings of these processes hinder the development of advanced, fiber-based micro-devices, particularly when precise, three-dimensional fiber orientations are required. Furthermore, wet and dry spinning are limited to microscale diameters (tens to hundreds of microns), while electrospinning is confined to the nanoscale (tens of nanometers to single microns).

Recently, a new class of processes has been developed by our group and others to overcome these constraints through directed self-assembly of suspended micro- and nanofibers. In one such process, a high-viscosity solution is loaded onto an applicator and manually brushed across an array of microfabricated pillars to form aligned air bridges of solution filaments. These filaments then thin, through surface tension-driven necking, and solidify, via evaporation, to yield aligned arrays of suspended nanofibers [12–14]. Variants of this process involve using an AFM cantilever [15] or micromanipulator-controlled stylus [16] to draw suspended filaments of polymer

* Corresponding author. Department of Bioengineering, 419 Lutz Hall, University of Louisville, Louisville, KY 40292, USA. Tel.: +1 502 852 6356; fax: +1 502 852 6806.
*E-mail addresses:* Scott.Michael.Berry@gmail.com (S.M. Berry), santosh.pabba@intel.com (S. Pabba), rob.keynton@louisville.edu (R.S. Keynton).
[1] Present address: Department of Biomedical Engineering, University of Wisconsin–Madison, 1111 Highland Ave., WIMR 6th Floor, Madison, WI 53726, USA.
[2] Present address: D1C Litho-Immersion Scanner, Intel Corporation, Hillsboro, OR, USA.

0032-3861/$ – see front matter © 2011 Elsevier Ltd. All rights reserved.
doi:10.1016/j.polymer.2011.01.059

solutions [16–18] or melts [15,19]. However, these processes all require the pre-deposition of polymeric material on either the substrate or the drawing stylus. Additionally, buildup of dried solution on the styli tip has been observed to induce an unwanted variation on fiber diameter when several fibers are drawn in series [16].

In an attempt to mitigate these variations, the stylus-drawing techniques have been modified into a "direct-write" process, in which the polymeric material is directly ejected from a hollow capillary and then drawn into filaments which thin and solidify (Fig. 1). Using this process, our group [16] and others [15] have produced polymer fibers with micro- and nanoscale diameters by employing this method. Nain et al. [20] also demonstrated limited control of fiber diameter by allowing the ejected droplet to dry for a period of time prior to drawing. Alternative direct-write embodiments that do not utilize surface tension-driven fluid mechanics to control diameter have also been reported in the literature [21,22].

Despite previous demonstrations of direct-write (and similar) fiber production, the mechanisms governing fiber formation are not well characterized and the parameters which influence direct-write success are not sufficiently defined to enable potential users to utilize the process without laborious trial-and-error optimization. In this investigation, we will characterize the direct-write process using a model system of poly(methyl methacrylate) (PMMA). The data generated will be analyzed to determine trends that relate fiber diameter to polymer solution properties and/or system geometry. Also, viscosity measurements and physical properties of the solution will be measured and utilized to build correlations between the fiber diameter and the governing dimensionless groups of the system. This empirical model of the direct-write process will then be validated by employing it to predict the diameters of fibers drawn from five other non-PMMA-based polymer/solvent systems.

## 2. Materials and methods

### 2.1. Theoretical models

In order to produce stable polymer fibers from a particular polymer solution, we must first understand the physics governing volatile liquid bridges. In a liquid bridge, stretching and surface tension-driven capillarity promote bridge thinning, while elasticity, viscosity, and inertia all act to mitigate these forces. Since the liquid bridges generated by the direct-write system are microscale and highly viscous, inertia is dominated by viscosity and can be neglected as confirmed by the low Reynolds numbers encountered in this study ($Re < 0.01$ in all experiments). Similarly, elastic effects were found to be negligible as evidenced by the low elastocapillary number ($Ec < 0.4$ in all experiments performed), suggesting that polymer chain relaxation occurs relatively quickly compared with capillary thinning. Upon inclusion of these simplifications, liquid bridge formation is governed only by surface tension-driven capillarity, stretching, and viscosity.

While the mechanics governing direct-write fiber formation have not been previously elucidated, the surface tension-driven thinning of a liquid bridge has been extensively studied. Here, we attempt to apply this established theory to the direct-write process by examining the assumptions and limitations of the previous models in order to determine their applicability to the direct-write process (An overview of the discussed models is given in Table 1). The thinning of a Newtonian liquid bridge between two fixed plates has been predicted to be a function of time, initial bridge diameter, and "capillary velocity", defined as the ratio of surface tension to viscosity [23–25]. However, Eq. (1) (see Table 1) suggests that as time increases, diameter decreases linearly and ultimately reaches zero, indicating break-up of the capillary.

The evaporation of the volatile solvent from the thinning capillary is necessary to asymptotically increase viscosity and promote the stabilization of liquid bridges into solid fibers. The inclusion of volatility complicates the capillary break-up model since solvent evaporation results in a significant increase in viscosity over the course of bridge thinning. Tripathi et al. [26] have developed a theory that accounts for the evaporation of a volatile solvent component of a polymer solution. This work suggests that the magnitude of thinning is related to a dimensionless "Processability Parameter" as described by Eqs. (2) and (3). Conceptually, Eq. (3) (see Table 1) can be interpreted as the ratio of the drying rate to the capillary velocity, which is related to the rate of surface tension-driven thinning of the liquid bridge. For a constant-length filament of Newtonain solution, Tripathi et al. suggest that fiber diameter will converge to a steady-state, non-zero value.

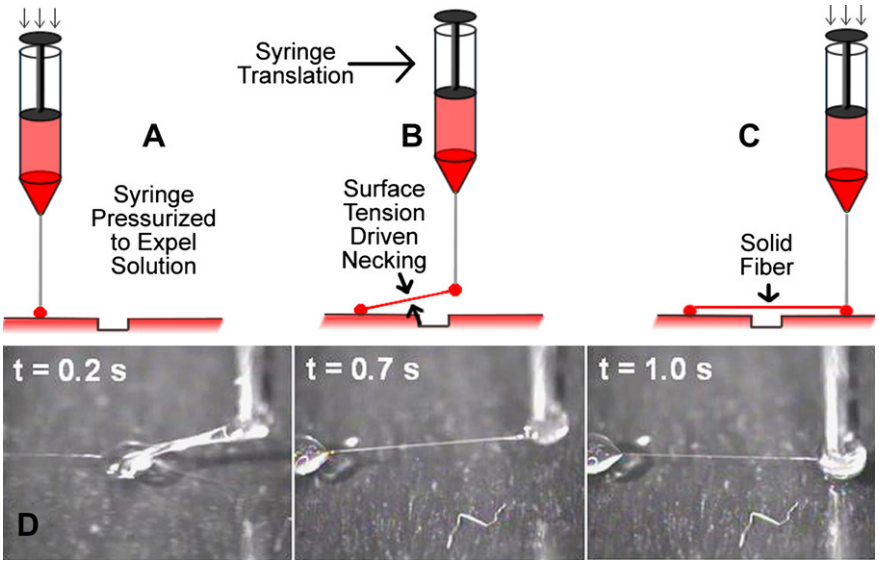


**Fig. 1.** Schematic illustrating the direct-write drawing of fibers from a polymer solution. A) Solution is expelled into contact with substrate. B) Syringe is translated to desired endpoint while the drawn polymer filament undergoes simultaneous capillary thinning and drying. C) Solution is expelled to establish second contact point, creating a suspended fiber. D) Actual images of fiber drawing process.

**Table 1**
Evolution of the mathematical models used to describe the relationship between fiber diameter, system geometry, and solution properties. D(t) is fiber diameter as a function of time, $D_1$ is fiber diameter immediately after formation of a liquid bridge, $X$ is a constant equal to 0.7127 [23], $\sigma$ is surface tension, $\eta$ is Newtonian viscosity, P is Processability Parameter, $\chi$ is solvent mass transfer coefficient, Ca is capillary number, $\Lambda$ is aspect ratio, U is fiber drawing velocity, $L$ is fiber length, and $D_0$ is solution droplet diameter prior to elongation. $D_0$ is assumed to equal the diameter of the capillary in the direct-write technique.

| Model | Assumptions | Equations | Refs. |
|---|---|---|---|
| Capillary break-up | Fixed length (No Stretcling), non-volatile, Newtonian | $D(t) = D_1 - \frac{(2X-1)}{3}\frac{\sigma}{\eta}t$ (1) | [23–25] |
| "Processability" parameter | Fixed length, Newtonian | $D(t=\infty) = D_1 e^{-0.0709/2P}$ (2)<br>$P = \frac{\eta\chi}{\sigma}$ (3) | [26] |
| Multi-parameter | Newtonian | $D(t=\infty) = f(p, Ca, \Lambda)$ $P = \frac{\eta\chi}{\sigma}Ca = \frac{\eta U}{\sigma}$ (4)<br>$\Lambda = \frac{L}{D_0}$ (5) | [27,28,30] |

While instantaneous (fixed length) and exponential stretching have been extensively described in the literature [27], linear stretching profiles such as the one applied by the direct-write system have been studied in relatively few cases [28]. The Processability Parameter model assumes the liquid bridge is formed instantaneously, such that the degree of bridge thinning is completely determined by capillarity and is independent of stretching. If formation of the bridge occurs at a finite drawing rate, U, stretching and capillarity will simultaneously act to thin the bridge, and therefore, both must be considered. For a Newtonian fluid, the resistance to stretching deformations is quantified by the extensional viscosity, which is consistently equal to three times the shear viscosity [29]. Therefore, it is unnecessary to add an additional term to the model to account for extensional viscosity when Newtonian behavior is assumed.

The degree of solution filament thinning can be expressed as a function of five variables: solution viscosity, solution surface tension, fiber length, drawing rate, and the mass transfer coefficient of the evaporating solvent (Fig. 2). Dimensional analysis suggests that the direct-write system can be correctly parameterized using three dimensionless parameters. In addition to the aforementioned Processability Parameter, two dimensionless parameters were defined to describe direct-write fiber diameter: capillary number (Ca, defined as Eq. (4) in Table 1) and aspect ratio ($\Lambda$, as defined in Eq. (5) in Table 1) [30]. Ca accounts for the non-instantaneous nature of the direct-write method, in which production of a single fiber can take a second or longer. Ca expresses the ratio of the drawing rate to the surface tension-driven thinning rate. A high Ca denotes a case where drawing occurs so rapidly that the majority of the surface tension-driven thinning occurs after extension is complete. Conversely, a case with low Ca experiences significant thinning (and possibly drying) during drawing, which may lead to further thinning or failure due to tensile stretching.

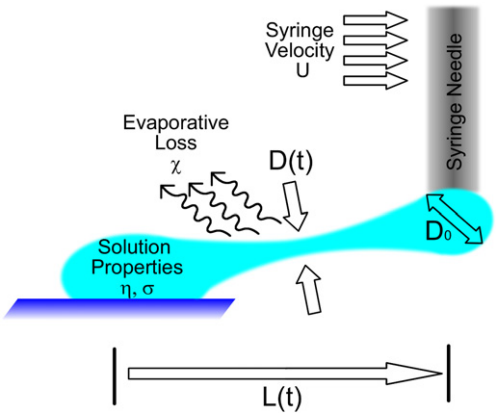


**Fig. 2.** Graphical representation of the relevant variables in the direct-write process.

In each of the models described in Table 1, including the multi-parameter model, non-Newtonian effects such as elasticity, strain hardening, or molecular extensibility were ignored. Rather, it is assumed that the polymer solutions possess nearly-constant capillary velocities, defined as $\sigma/\eta$, over the course of liquid bridge thinning. Mathematically, this qualification is characterized by a linear ($R^2$ to linear fit $> 0.95$) relationship between filament diameter and time for a constant-length polymer filament, as is expressed by Eq. (1). This relationship is illustrated conceptually for both Newtonian-like (linear) and non-Newtonian (non-linear) polymer solutions in Section 3.2, where we will justify the assumption that the PMMA model system behaves as a Newtonian-like liquid, thus enabling us to apply the multi-parameter model to our data.

### 2.2. Solution preparation

PMMA solutions were produced by dissolving PMMA homopolymer (996 kDa, Sigma–Aldrich, St. Louis, MO) in chlorobenzene at concentrations of 22%, 23%, 24%, 25%, and 26% by weight. The non-PMMA-based polymer solutions were created by dissolving a variety of different biodegradable polymers (all obtained from Durect, Cupertino, CA) in organic solvents as indicated in Table 2. These solvents were selected from a library of common polymer solvents based on two criteria derived during preliminary experimentation: 1) The capability of the solvent to dissolve the polymer within a range of concentrations sufficient for direct-write (22%–32% by weight), and 2) Possession of a moderate volatility as defined by a boiling point ranging from 80 to 140 °C. It should be noted that chloroform does not satisfy the second criterion (b.p. = 61 °C), but no other suitable solvent could be identified for the L-PLA polymer.

### 2.3. Direct-write of PMMA fibers

PMMA test solutions were drawn into arrays of fibers using the direct-write technique illustrated in Fig. 1. In this process, a syringe was loaded with polymer solution and affixed to a programmable, ultra-high precision micromilling machine (MMM) (Dover Instrument Corp.) with a lateral resolution of 1.25 nm and a vertical resolution of 20 nm. The tip of the syringe needle was positioned 500 μm above a glass substrate and continuously pressurized with weights to expel PMMA solution from a 22 gauge needle (I.D. = 394 μm) at a rate of ~20 μL/min until a pendant droplet of solution contacted the substrate. The syringe was then lifted 1 mm and translated laterally, drawing this droplet into a filament of solution, which thinned via surface tension-driven necking. Additional contact points were produced in a "connect-the-dots" fashion by lowering the syringe such that the pendant droplet made contact with substrate. Meanwhile, solvent evaporation from the thinning filaments caused the formation of solidified fibers, assuming that evaporation occurs sufficiently fast to avoid capillary breakup of the filaments.

**Table 2**
Polymer test solutions.

| Polymer | Abbreviation | Intrinsic viscosity (dL/g) | Solvent | Tested mass fractions |
|---|---|---|---|---|
| Poly(methyl methacrylate) | PMMA | 1.25 | Chlorobenzene | 22%–26% |
| Poly(L-lactide) | L-PLA | 0.90–1.20 | Chloroform | 28%, 29% |
| Poly(DL-lactide) | DL-PLA | 0.55–0.75 | 1,2 Dichloroethane | 30%, 32% |
| 50:50 Poly(DL-lactide-co-glycolide) | 50:50 DL-PLGA | 0.76–0.94 | 1,2 Dichloroethane | 22.5%, 23% |
| 75:25 Poly(DL-lactide-co-glycolide) | 75:25 DL-PLGA | 0.55–0.75 | Chlorobenzene | 29%, 30% |
| Poly(caprolactone) | PCL | 1.00–1.30 | 1,2 Dichloroethane | 28%, 30% |

Fibers were drawn from each of the five PMMA test solution concentrations at velocities of 5 and 20 mm/s to lengths ranging from 2 mm to 20 mm in 2 mm increments. After coating with a thin layer ($t \approx 10$ nm) of gold-palladium alloy, all fibers were imaged using a scanning electron microscope (SEM) (Zeiss Supra 35VP, Thornwood, NY). Diameter measurements were recorded at the middle of each fiber as well as 200 μm from each end. Analysis of variance (ANOVA) and Student's *T*-test were employed to determine the statistical significance of any apparent trends.

### 2.4. Solution characterization

The surface tensions of the solutions were measured using the Wilhelmy technique. Specifically, a glass rod (diameter = 4.3 mm) was dipped into each solution and the force exerted on the rod due to surface tension was measured with a balance. A micromanipulator was utilized to precisely position the tip of the rod at the surface of the solution such that the force due to the buoyancy of the rod was negligible. This measured force, F, is related to surface tension, $\sigma$, by:

$$\sigma = \frac{F}{s\cos\theta} \tag{6}$$

where, $s$ is the perimeter of the rod ($s = 13.5$ mm) and $\theta$ is the contact angle of the fluid on the rod. Glass was chosen as the rod material since all test solutions were found to wet glass completely such that $\theta$ approached 0° [31].

Solution viscosities were measured using the capillary breakup rheometer (CaBER). This instrument stretches a cylinder of solution into a filament in a nearly-instantaneous manner ($t_{stretch} = 20$ ms), then monitors the diameter of the filament midpoint as it thins due to capillary action. This diameter, $D_{mid}(t)$, is related to Newtonian viscosity and surface tension by Eq. (1) [32].

The drying rates of the polymer solutions were quantified by measuring the mass transfer coefficient of the solvents from the solutions in an atmosphere of air at room temperature. The mass of the solution, m($t$), was monitored by thermogravimetric analysis (TGA, TA Instruments TGA 2950, New Castle, DE) and the mass transfer coefficient, $\chi$, was then calculated as:

$$\chi = \frac{-\dot{m}(t)}{Ac(t)} \tag{7}$$

where $c(t)$ is the concentration of the solvent (in kg/L) and $A$ is the area of the solution/air interface ($A = 78.5$ mm$^2$ for standard TGA plate). Concentration was determined from $m(t)$ by:

$$c(t) = \frac{m(t) - m_{POLYMER}}{V(t)} \tag{8}$$

where $m_{POLYMER}$ is the mass of the polymer in the solution and V($t$) is the solution volume, which was calculated by:

$$V(t) = \frac{m(t)}{\rho} \tag{9}$$

where $\rho$ is the density of the solution, which was assumed to be constant over the course of the drying experiment.

### 2.5. Empirical model generation

The solution properties were combined with the direct-write system geometry to calculate a series of dimensionless parameters which describe the thinning and solidification behaviors of a filament of polymer solution. An empirical model linking fiber diameter to the dimensionless parameters P, Λ, and Ca was generated by calculating a statistical fit via Maple Software (Waterloo) using the characterization data for PMMA outlined in Section 2.4. This model was then visualized by the production of a series of surface and contour plots. Statistical tools including ANOVA and *T*-test were then utilized to identify any significant relationships between the dimensionless variables and the direct-write process outcomes.

### 2.6. Validation of empirical model

The empirical model expresses the fiber diameter in terms of the variables which directly influence the mechanics of fiber formation as described in Section 2.1. Therefore, assuming the model encompasses all variables which significantly affect fiber formation; it can be accurately employed to predict the direct-write production of fibers from a *general* polymer solution in addition to

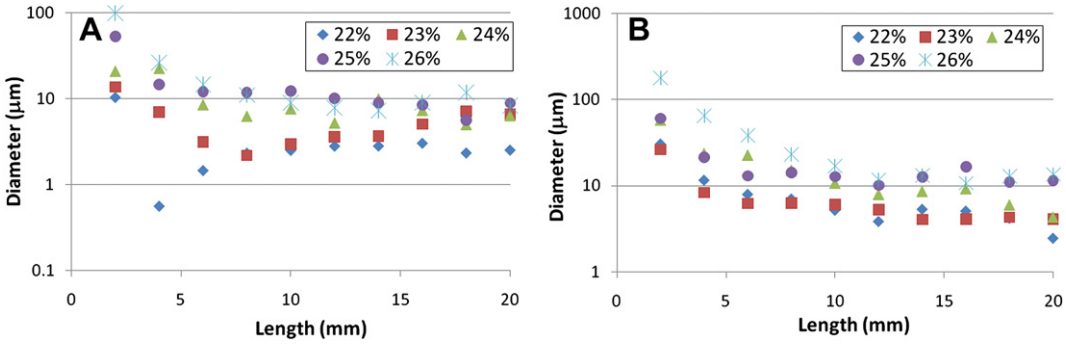


**Fig. 3.** Diameter versus length for direct-writing of PMMA (MW = 996 kDa) fibers drawn at A) 5 mm/s and B) 20 mm/s with the 22 gauge needle.

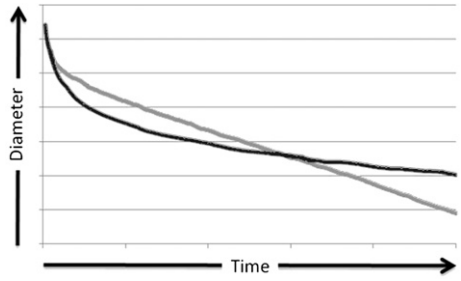


**Fig. 4.** Capillary thinning of constant-length filaments of "Newtonian-like" PMMA solution (MW = 996 kDa) (light line) and non-Newtonian PMMA solution with 1.5% carbon nanotubes (dark line). Data were collected via capillary breakup rheometry (HAAKE CaBER 1 Extensional Rheometer, Thermo Scientific, Waltham, MA) and axes are in linear space.

the specific PMMA/chlorobenzene solutions which were used to generate the model. This assumption was tested by drawing fibers from the remainder of the materials described in Table 2 and comparing the diameters of these fibers with the values predicted by the model.

Fibers with lengths of 4, 8, and 16 mm were drawn at a rate of 20 mm/s from all solutions listed in Table 2 with the direct-write system (Figs. 1 and 8) drawing attempts were made at each length for each solution. Fibers were metalized and measured via SEM as previously described. Viscosities, surface tensions, and mass transfer coefficients were measured for each solution as previously described and used to calculate P, Λ, and Ca. The values of these three dimensionless parameters were then utilized in conjunction with the empirical model to generate fiber diameter predictions for each solution, which were then compared against the experimental results.

## 3. Results

### 3.1. Direct-write of PMMA fibers

PMMA fibers with diameters ranging from 400 nm to over 100 μm were successfully produced with the direct-write system. It was discovered that fiber diameter increases significantly with increasing concentration ($p < 0.001$) and decreasing fiber length ($p < 0.001$), but the drawing rate does not significantly affect diameter ($p = 0.15$). These trends are illustrated in Fig. 3, which presents fiber diameter as a function of concentration and length for drawing rates of 5 and 20 mm/s. We observed that many fibers fractured when drawing at a slower speed (1 mm/s) or with a smaller needle (26s gauge, I.D. = 114 μm) due to excessive drying before or during the elongation process. Additionally, fiber diameter was smallest at the axial midpoint ($p < 0.005$ compared with measurements near the fiber endpoints) and smaller at the end

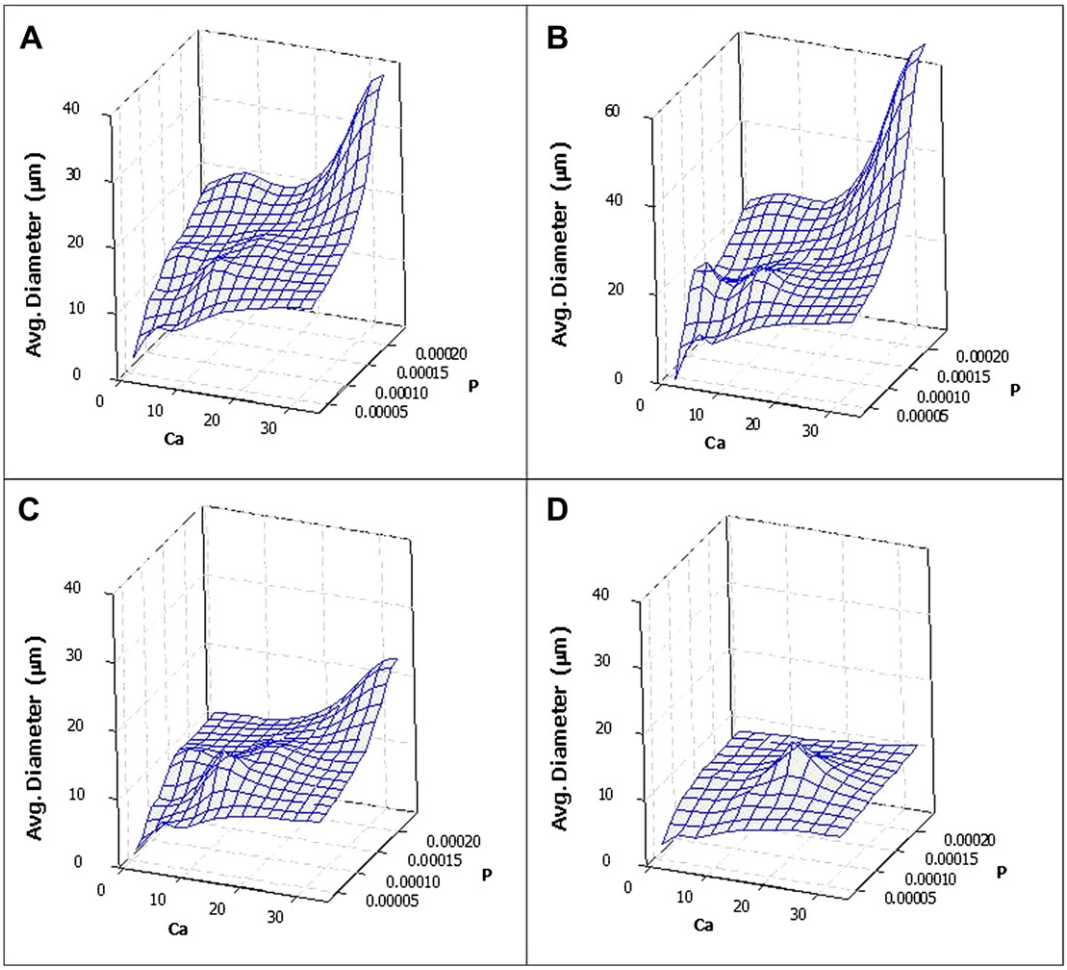


**Fig. 5.** Diameter as a function of P and Ca for fibers drawn from PMMA solutions (996 kDa). A) Averaged data for all tested lengths (2–20 mm in 2 mm increments), B) Data for fiber length of 4 mm, C) Data for fiber length of 8 mm, and D) Data for fiber length of 16 mm. Note that the 4 mm data has a different vertical scale than the other surfaces.

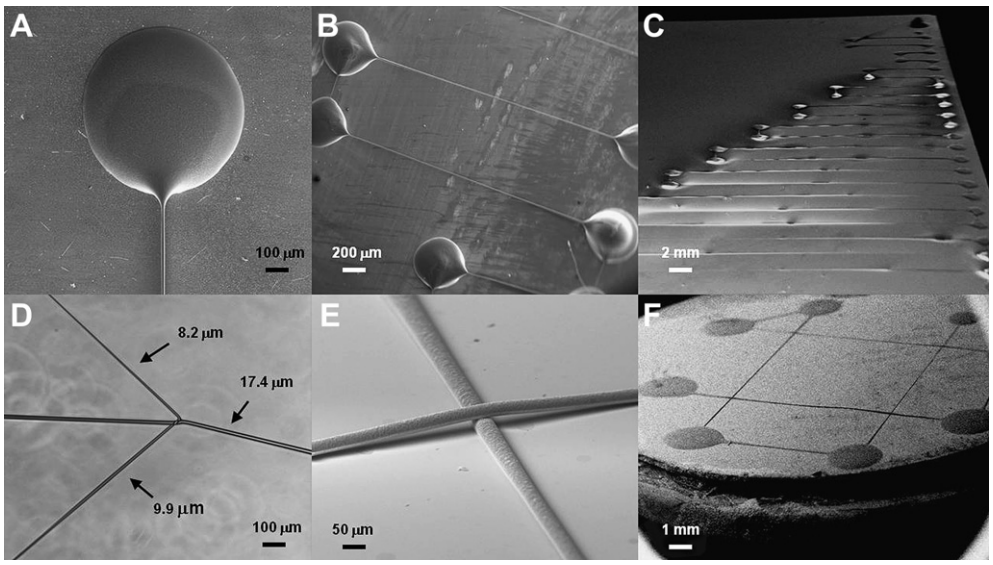


**Fig. 6.** SEM images of representative fibers fabricated with the direct-write system. A) End of PCL fiber, B) Array of 50:50 PLGA fibers, C) Isometric view of array of PMMA fibers of increasing length, D) Suspended, branched 50:50 PLGA structure with diameter measurements, E) Overlapping 75:25 PLGA fibers, and F) Array of overlapping 75:25 PLGA fibers.

where drawing was initiated than at the end where drawing was terminated ($p < 0.001$; Average coefficient of variation along length of fiber = 38%). The diameters of multiple fibers drawn with identical experimental parameters exhibited an average coefficient of variation of 46%.

### 3.2. PMMA solution characterization

The surface tensions of the five PMMA solutions were measured using the Wilhelmy technique. ANOVA analysis of this data demonstrated that PMMA concentration does not significantly affect surface tension ($p = 0.66$). The capillary velocities of the solutions decreased with increasing concentrations, while viscosity was observed to increase with increasing concentration (Table 3). The solution evaporation coefficient, which is independent of concentration, was measured via TGA to have a value of $1.06 \times 10^{-7}$ m/s with a standard deviation of $1.61 \times 10^{-8}$ m/s.

The thinning of the PMMA solution filaments was measured as a function of time with the CaBER instrument to determine the linearity of $\sigma/\eta$, which is a signature of Newtonian-like behavior (Eq. (1)). Fig. 4 shows data from a PMMA solution compared to data from a known non-Newtonian system (PMMA spiked with 1.5% carbon nanotubes). Fig. 4 illustrates the difference between the thinning behaviors of these two systems and suggests that the PMMA solution can be modeled as a Newtonian system (with regard to thinning) due to its linearity ($R^2$ of linear fit is 0.996). The effect of drying is not apparent in Fig. 4 (i.e., diameter does not reach steady-state) as the diameter of the solidified bridge is below the detection level of the rheometer.

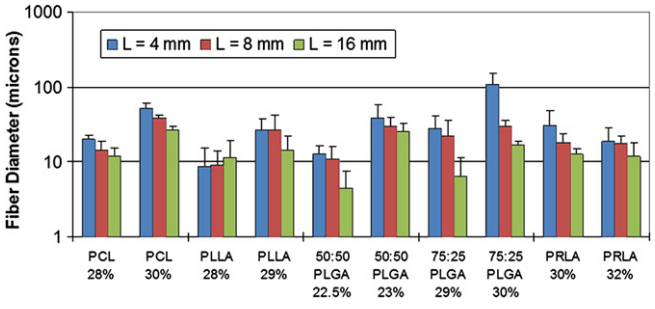


**Fig. 7.** Diameters of biodegradable fibers produced with the direct-write system.

### 3.3. Empirical model generation

The solution property data expressed in Table 2 was utilized in conjunction with Eqs. (3) and (4) to calculate values of the Processability Parameter, P, and the capillary number, Ca, for each PMMA solution/drawing rate combination (Table 4). It was revealed that fiber diameter increased with increasing values of both the Processability Parameter ($p < 0.005$) and the capillary number ($p < 0.02$). A series of surface plots describing this relationship is given as Fig. 5, which can be approximated by the third-order polynomial:

$$D(t) = 1.41Ca - 0.074Ca^2 + 0.016Ca^3 + 60469P - 7.65\Lambda + 0.24\Lambda^2 - 0.0023\Lambda^3 + 69.008 \quad (10)$$

It should be noted that the higher order terms associated with P were negligibly small and were therefore excluded from Eq. (10).

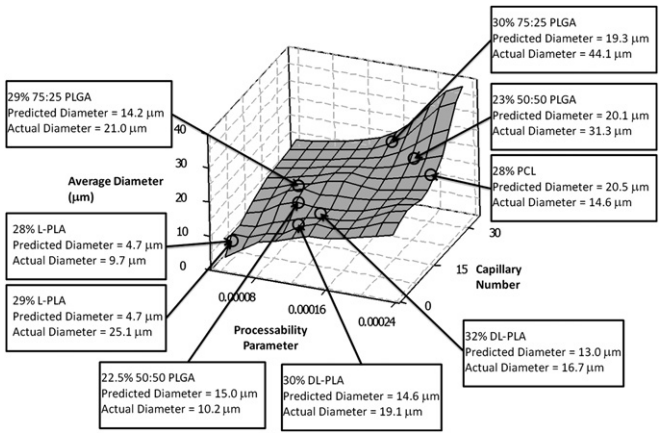


**Fig. 8.** Comparison of the average diameter in the state space P – Ca for biodegradable polymer solutions with the reference surface for PMMA fibers (Fig. 5a).

**Table 3**
PMMA solution properties.

| PMMA conc. | Surface tension (mN/m) | Capillary velocity (m/s) | Viscosity (Pa*s) |
|---|---|---|---|
| 22% | 42.90 ± 8.45 | 3.456 ± 0.326 | 12.50 ± 1.24 |
| 23% | 41.42 ± 4.03 | 3.115 ± 0.438 | 13.49 ± 2.06 |
| 24% | 37.16 ± 7.26 | 1.486 ± 0.071 | 25.06 ± 1.21 |
| 25% | 42.78 ± 4.41 | 1.070 ± 0.187 | 40.76 ± 6.53 |
| 26% | 43.58 ± 7.23 | 0.609 ± 0.086 | 72.61 ± 10.83 |

**Table 4**
Dimensionless parameters for PMMA solutions.

| PMMA conc. | P | Ca @ 5 mm/s | Ca @ 20 mm/s |
|---|---|---|---|
| 22% | $3.1 \times 10^{-5}$ | 0.94 | 3.77 |
| 23% | $3.4 \times 10^{-5}$ | 1.55 | 6.21 |
| 24% | $7.1 \times 10^{-5}$ | 2.76 | 11.03 |
| 25% | $9.9 \times 10^{-5}$ | 3.81 | 15.25 |
| 26% | $17.4 \times 10^{-5}$ | 5.96 | 23.84 |

The average error between the experimental data and this model is 7.63 μm, or 53%, which is similar in magnitude to the coefficient of variation (46%) for this data.

### 3.4. Direct-write of fibers from non-PMMA-based polymers

The versatility of the direct-write process was demonstrated by processing a variety of non-PMMA-based polymer/solvent pairs (as described in Table 2) into microscale fibers (Fig. 6). The general trends observed with the PMMA solutions describing the relationships between fiber diameter, polymer concentration, and fiber length appear to be conserved as illustrated by Fig. 7. In all cases, except the two L-PLA solutions, fiber diameter significantly decreased as length increased. Likewise, fiber diameter increased with increasing polymer concentration in all cases excluding DL-PLA. Unbroken fibers were typically produced with all solutions listed in Table 2, with exception of the 29% 75:25 DL-PLGA, which often experienced capillary breakup due to excessive surface tension, and the two L-PLA solutions, which partially dried during the drawing process due to the high volatility of chloroform.

### 3.5. Validation of empirical model

Viscosity, surface tension, and solvent mass transfer coefficient were measured and used to calculate Processability Parameter and capillary number for the biodegradable polymers (Table 5). It should be noted that, although successfully processed into fibers with the direct-write system, the 30% PCL solution possessed a value for P that was well in excess of the characterized range reported in Table 3 (approximately $0–17 \times 10^{-5}$). Therefore, predictions for this material could not be enumerated and it was omitted from the empirical model validation. Additionally, all solutions were observed to thin at a relatively constant rate as evidenced by the highly-linear relationships ($R^2 > 0.97$) between solution filament diameter and time, suggesting that the capillary thinning behavior of these particular solutions is approximately Newtonian in nature.

Calculated values of P and Ca for the biodegradable polymer solutions were used to plot these solutions on the surface of the surface plot (Fig. 5) relating PMMA fiber diameter to P and Ca (Fig. 8). Additionally, values of P, Ca, and Λ were utilized to develop fiber diameter predictions based on Fig. 5 and Eq. (10). The error between the biodegradable fiber diameter predictions to the actual diameters are given in Table 5. The accuracy of the empirical model for predicting fiber diameter varies significantly across the five biodegradable materials. While the majority of the predictions fall within 50% of the actual values, the predictions for the two L-PLA solutions consistently deviate substantially from actual data. These errors are likely a consequence of the volatile nature of the chloroform, which partially evaporates during the direct-write setup time of 5–10 min. Since the direct-write fiber diameter was shown to be strongly influenced by solution concentration (2.6-fold increase in diameter between 28% and 29% L-PLA solutions), any loss of solvent would consequently increase the diameters of any fabricated fibers. The empirical predictions, which were derived from solution characterization measurements with shorter setup times (3–5 min), experienced smaller exaggerations and were, therefore, substantially lower than the actual direct-write data. By removing the L-PLA data, the prediction error dropped from 46% to 38%, resulting in an average absolute error of 8.8 μm, considering an average fiber diameter of 23.3 μm.

## 4. Discussion

Careful control of the stretching rate, the final aspect ratio, and the rate of capillary thinning and drying is necessary during the direct-write process to avoid breakup and reach a desired equilibrium diameter. Each solution must possess sufficient surface tension to shape liquid filaments into the desired microscale structures, sufficient viscosity to resist capillary breakup, and sufficient volatility to promote solidification of the fiber. Those parameters can be compactly represented using three dimensionless groups in the case of Newtonian fluids. If this balance is disrupted, stable microscale fibers will no longer be produced. This effect becomes evident when the concentration of a solution is modified, thereby substantially altering viscosity without significantly affecting surface tension or volatility. Indeed, several concentrations outside the ranges given in Table 2 were tested, and it was discovered that concentrations below these ranges always resulted in capillary breakup while those above the ranges produced macroscale (>100 μm) fibers with irregular cross-sections.

**Table 5**
Physical properties and dimensionless parameters for biodegradable polymer solutions. The shaded value of P indicates a level that fell outside the boundaries of the PMMA-based empirical model.

| Solution | Surface tension (mN/m) | Viscosity (Pa*s) | Evaporation coef. (m/s) | $R^2$ of linear Fit | P | Ca | Prediction error |
|---|---|---|---|---|---|---|---|
| 28% PCL | 55.7 ± 10.6 | 27.9 ± 7.1 | $5.26 \times 10^{-7}$ | 0.998 | $26 \times 10^{-5}$ | 10.02 | 25.9% |
| 30% PCL | 56.9 ± 5.6 | 71.9 ± 9.8 | $5.26 \times 10^{-7}$ | 0.990 | $66 \times 10^{-5}$ | 25.27 | NA |
| 28% L-PLA | 46.7 ± 0.4 | 3.1 ± 1.0 | $3.62 \times 10^{-7}$ | 0.974 | $2.4 \times 10^{-5}$ | 1.33 | 59.7% |
| 29% L-PLA | 53.8 ± 17.2 | 3.6 ± 2.0 | $3.62 \times 10^{-7}$ | 0.970 | $2.4 \times 10^{-5}$ | 1.34 | 83.9% |
| 22.5% 50:50 DL-PLGA | 51.1 ± 1.8 | 20.6 ± 5.2 | $2.18 \times 10^{-7}$ | 0.993 | $8.8 \times 10^{-5}$ | 8.06 | 38.5% |
| 23% 50:50 DL-PLGA | 47.2 ± 1.9 | 45.9 ± 9.3 | $2.18 \times 10^{-7}$ | 0.973 | $21 \times 10^{-5}$ | 19.45 | 46.9% |
| 29% 75:25 DL-PLGA | 107.1 ± 17.6 | 69.9 ± 24.0 | $1.31 \times 10^{-7}$ | 0.998 | $8.5 \times 10^{-5}$ | 13.05 | 31.3% |
| 30% 75:25 DL-PLGA | 70.7 ± 6.6 | 88.4 ± 19.1 | $1.31 \times 10^{-7}$ | 0.991 | $16 \times 10^{-5}$ | 25.01 | 49.7% |
| 30% DL-PLA | 56.2 ± 3.3 | 15.3 ± 7.3 | $4.43 \times 10^{-7}$ | 0.993 | $12 \times 10^{-5}$ | 5.44 | 45.5% |
| 32% DL-PLA | 53.0 ± 0.0 | 16.5 ± 3.4 | $4.43 \times 10^{-7}$ | 0.991 | $14 \times 10^{-5}$ | 6.23 | 30.2% |

Although the workable concentration range for a given material is quite narrow in the tested cases (~1–5%), the necessary rheological conditions for fiber fabrication were found to be relatively conserved, enabling the construction of a general empirical model to aid in the accurate customization of new material solutions and eliminating the need for trial-and-error characterization. This model (Eq. (10) and Fig. 5) can be utilized to design solutions which will repeatably form fibers with predictable diameters. The average error of these predictions was measured to be 46% for the series of biodegradable polymers, which is identical to the coefficient of variation of the diameters of the PMMA fibers employed to generate the model. This observation indicates that the error in predicting the biodegradable fiber diameters is equal to the error intrinsic to the model due to the variability of the PMMA fiber diameters, suggesting that the model predicts both classes of materials with nearly equal accuracy. This ability to apply a model generated from a common polymer (PMMA) to polymers with specialized properties, such as biodegradability, potentially facilitates the direct-write production of suspended fibers with a wide variety of customizable properties without the need for lengthy trial-and-error characterization.

## 5. Conclusions

A newly-developed direct-write system was utilized to produce arrays of suspended micro and sub-microscale polymer fibers. Fibers composed of PMMA and several biodegradable polymers were fabricated with this process in a variety of precisely-positioned, three-dimensional arrangements. In general, it was discovered that fiber diameter increased with increasing polymer concentration as well as decreasing fiber length, while remaining unchanged as drawing velocity was modified.

The polymer concentration range where direct-write drawing is possible (i.e., unbroken, suspended fibers) was generally quite narrow (<5%) and typically varied from polymer to polymer. Attempts to produce fibers from solutions with concentrations outside of these ranges were not successful. Initially, determination of the workable concentration range entailed lengthy trial-and-error characterizations. However, to circumvent this laborious analysis, a generalized empirical model was generated using data from a series of PMMA/chlorobenzene solutions. This model expressed fiber diameter in terms of three dimensionless parameters defined by fundamental rheological factors that directly influence the thinning and solidification of a filament of viscous polymer solution.

To test the accuracy of the empirical model, it was employed to elucidate “predictions” for the diameters of fibers drawn from solutions of various biodegradable polymers including L-PLA, DL-PLA, PCL, 50:50 PLGA, and 75:25 PLGA. These solutions possessed significantly different viscosities, surface tensions, and evaporation rates compared to the PMMA solutions. However, once these properties were packaged into the aforementioned dimensionless parameters and used in conjunction with the empirical model to enumerate the predictions, it was discovered that the predicted values fell within 46% of the actual data. This error declined to 38% when the outlying L-PLA data was removed since it experienced significant uncontrolled drying prior to fiber drawing due to the high volatility of its solvent (chloroform).

## Acknowledgments

This investigation was funded by National Science Foundation NIRT Program (ECS-0506941), NSF PFI Program (EEC-0438604), and "National Aeronautics and Space Administration cooperative agreement (NCC5-571).

## References

[1] Cho SM, Kim YJ, Kim YS, Yang Y, Ha S-C. The application of carbon nanotube-polymer composite as gas sensing materials. Sensors, 2004. Proceedings of IEEE; 2004.
[2] Xu F, Horak P, Brambilla G. Optical microfiber coil resonator refractometric sensor. Optics Express 2007;15(12):7888–93.
[3] Dalton PD, Joergensen NT, Groll J, Moeller M. Patterned melt electrospun substrates for tissue engineering. Biomedical Materials 2008;3(3):11.
[4] Ekaputra AK, Prestwich GD, Cool SM, Hutmacher DW. Combining electrospun scaffolds with electrosprayed hydrogels leads to three-dimensional cellularization of hybrid constructs. Biomacromolecules 2008;9(8):2097–103.
[5] Hadjizadeh A, Doillon CJ, Vermette P. Bioactive polymer fibers to direct endothelial cell growth in a three-dimensional environment. Biomacromolecules 2007;8:864–73.
[6] Xu CY, Inai R, Kotaki M, Ramakrishna S. Aligned biodegradable nanofibrous structure: a potential scaffold for blood vessel engineering. Biomaterials 2004;25:877–86.
[7] You Y, Min B-M, Lee SJ, Lee TS, Park WH. In vitro degradation behavior of electrospun polyglycolide, polylactide, and poly(lactide-co-glycolide). Journal of Applied Polymer Science 2005;95:193–200.
[8] Berry SM, Warren SP, Hilgart DA, Schworer AT, Pabba S, Gobin AS, et al. Endothelial cell scaffolds generated by 3D direct writing of biodegradable polymer microfibers. Biomaterials 2011;32:1872–9.
[9] Dalton AB, Collins S, Munoz E, Razal JM, Ebron VH, Ferraris JP, et al. Super-tough carbon-nanotube fibres. Nature 2003;423:703.
[10] Dalton AB, Collins S, Razal JM, Munoz E, Ebron VH, Kim BG, et al. Continuous carbon nanotube composite fibers: properties, potential applications, and problems. Journal of Materials Chemistry 2004;14:1–3.
[11] Sperling LH. Introduction to physical polymer science. 3 ed. Wiley-Interscience; 2001.
[12] Harfenist SA, Cambron AD, Nelson EW, Berry SM, Isham AW, Crain MM, et al. Direct drawing of suspended filamentary micro- and nanostructures from liquid polymers. Nano Letters 2004;4(10):1931–7.
[13] Pabba S, Sidorov AN, Berry SM, Yazdanpanah MM, Keynton RS, Sumanasekera GU, et al. Oriented nanomaterial air-bridges formed from suspended polymer-composite nanofibers. ACS Nano 2007;1(1):52–67.
[14] Pabba S, Yazdanpanah MM, Fasciotto Totten BH, Dobrokhotov VV, Rathfon JM, Tew GN, et al. Biopolymerization-driven self-assembly of nanofiber air-bridges. Soft Matter 2009;5(7):1378–85.
[15] Nain AS, Amon C, Sitti M. Three-dimensional nanoscale manipulation and manufacturing using proximal probes: controlles pulling of polymer micro/nanofibers. IEEE; 2004.
[16] Berry SM, Harfenist SA, Cohn RW, Keynton RS. Characterization of micromanipulator-controlled dry spinning of micro- and sub-microscale polymer fibers. Journal of Micromechanics and Microengineering 2006;16:1825–32.
[17] CaBER Instruction Manual: Thermo Electron Corp.
[18] Berry SM, Harfenist SA, Cohn RW, Keynton RS. Characterization of micromanipulator controlled dry spinning of micro- and nanoscale polymer fibers. Oahu, Hawaii: MMB; 2005.
[19] Nain AS, Sitti M. 3-D nano-fiber manufacturing by controlled pulling of liquid polymers using nano-probes. IEEE; 2003.
[20] Nain AS, Wong JC, Amon C, Sitti M. Drawing suspended polymer micro-/-nanofibers using glass micropipettes. Applied Physics Letters 2006;89:183105.
[21] Vozzi G, Flaim C, Ahluwalia A, Bhatia S. Fabrication of PLGA scaffolds using soft lithography and microsyringe deposition. Biomaterials 2003;24:2533–40.
[22] Gratson GM, Xu M, Lewis JA. Direct writing of three-dimensional webs. Nature 2004;428:386.
[23] Kolte MI, Szabo P. Capillary thinning of polymeric filaments. Journal of Rheology 1999;43(3):609–25.
[24] Renardy M. A numerical study of the asymptotic evolution and breakup of Newtonian and viscoelastic jets. Journal of Non-Newtonian Fluid Mechanics 1995;59(2–3):267–82.
[25] Papageorgiou DT. On the breakup of viscous liquid threads. Physics of Fluids 1995;7(7):1529–44.
[26] Tripathi A, Whittingstall P, McKinley GH. Using filament stretching rheometry to predict strand formation and “processability” in adhesives and other non-newtonian fluids. Rheol Acta 2000;39:321–37.
[27] McKinley GH, Sridhar T. Filament-stretching rheometry of complex fluids. Annual Review of Fluid Mechanics 2002;34(1):375–415.
[28] Zhang X, Padgett RS, Basaran OA. Nonlinear deformation and breakup of stretching liquid bridges. Journal of Fluid Mechanics 1996;329:207–45.
[29] Trouton FT. On the coefficient of viscous traction and its relation to that of viscosity. Proceedings of the Royal Society of London Series A 1906;77:426–40.
[30] Crest J. Master thesis: formation of microfibers and nanofibers by capillary-driven thinning of drying viscoelastic filaments. Massachusetts Institute of Technology; 2009.
[31] de Gennes P-G, Brochard-Wyart F, Quere D. Capillarity and wettuing phenomena: drops, bubbles, pearls, waves. Springer; 2004.
[32] McKinley GH, Tripathi A. How to extract the Newtonian viscosity from capillary breakup measurements in a filament rheometer. Journal of Rheology 2000;44(3):653–70.